Spectral phasor analysis allows rapid and reliable unmixing of fluorescence microscopy spectral images

Farzad Fereidouni,[1] Arjen N. Bader,[1,2] and Hans C. Gerritsen[1,*]

[1]*Department of Molecular Biophysics, Debye Institute, Utrecht University, Utrecht, The Netherlands*
[2]*Crystal and Structural Chemistry, Bijvoet Centre, Utrecht University, Utrecht, The Netherlands*
[*]*H.C.Gerritsen@uu.nl*

Abstract: A new global analysis algorithm to analyse (hyper-) spectral images is presented. It is based on the phasor representation that has been demonstrated to be very powerful for the analysis of lifetime imaging data. In spectral phasor analysis the fluorescence spectrum of each pixel in the image is Fourier transformed. Next, the real and imaginary components of the first harmonic of the transform are employed as X and Y coordinates in a scatter (spectral phasor) plot. Importantly, the spectral phasor representation allows for rapid (real time) semi-blind spectral unmixing of up to three components in the image. This is demonstrated on slides with fixed cells containing three fluorescent labels. In addition the method is used to analyse autofluorescence of cells in a fresh grass blade. It is shown that the spectral phasor approach is compatible with spectral imaging data recorded with a low number of spectral channels.

OCIS codes: (170.2520) Fluorescence microscopy; (110.4234) Multispectral and hyperspectral imaging ;(110.2960) Image analysis.

References and links

1. J. Pawley, ed., *Handbook of Biological Confocal Microscopy* (Springer, 2006).
2. T. Zimmermann, J. Rietdorf, and R. Pepperkok, "Spectral imaging and its applications in live cell microscopy," FEBS Lett. **546**(1), 87–92 (2003).
3. Y. Garini, I. T. Young, and G. McNamara, "Spectral imaging: principles and applications," Cytometry A **69A**(8), 735–747 (2006).
4. H. C. Gerritsen, A. V. Agronskaia, A. N. Bader, and A. Esposito, "Time domain FLIM: Theory, instrumentation, and data analysis, " in *FRET and FLIM techniques,* T. W. J. Gadella, ed. (Elsevier, 2009), 95–132.
5. P. J. Verveer and Q. S. Hanley, "Frequency domain FLIM theory, instrumentation, and data analysis," in *FRET and FLIM Techniques,* T. W. J. Gadella, ed. (Elsevier, 2009), pp. 59–94.
6. P. I. H. Bastiaens and A. Squire, "Fluorescence lifetime imaging microscopy: spatial resolution of biochemical processes in the cell," Trends Cell Biol. **9**(2), 48–52 (1999).
7. J. Willem Borst and A. J. W. G. Visser, "Fluorescence lifetime imaging microscopy in life sciences," Meas. Sci. Technol. **21**(10), 102002 (2010).
8. V. E. Centonze, M. Sun, A. Masuda, H. Gerritsen, and B. Herman, "Fluorescence resonance energy transfer imaging microscopy," Methods Enzymol. **360**, 542–560 (2003).
9. A. N. Bader, A. M. Pena, C. Johan van Voskuilen, J. A. Palero, F. Leroy, A. Colonna, and H. C. Gerritsen, "Fast nonlinear spectral microscopy of in vivo human skin," Biomed. Opt. Express **2**(2), 365–373 (2011).
10. J. A. Palero, G. Latouche, H. S. de Bruijn, A. van der Ploeg van den Heuvel, H. J. Sterenborg, and H. C. Gerritsen, "Design and implementation of a sensitive high-resolution nonlinear spectral imaging microscope," J. Biomed. Opt. **13**(4), 044019 (2008).
11. R. A. Neher, M. Mitkovski, F. Kirchhoff, E. Neher, F. J. Theis, and A. Zeug, "Blind source separation techniques for the decomposition of multiply labeled fluorescence images," Biophys. J. **96**(9), 3791–3800 (2009).
12. D. M. Jameson, E. Gratton, and R. Hall, "The measurement and analysis of heterogeneous emissions by multifrequency phase and modulation fluorometry," Appl. Spectrosc. Rev. **20**(1), 55–106 (1984).
13. P. J. Verveer, A. Squire, and P. I. H. Bastiaens, "Global analysis of fluorescence lifetime imaging microscopy data," Biophys. J. **78**(4), 2127–2137 (2000).
14. G. I. Redford and R. M. Clegg, "Polar plot representation for frequency-domain analysis of fluorescence lifetimes," J. Fluoresc. **15**(5), 805–815 (2005).

#164083 - $15.00 USD Received 5 Mar 2012; revised 11 Apr 2012; accepted 11 Apr 2012; published 22 May 2012

15. M. A. Digman, V. R. Caiolfa, M. Zamai, and E. Gratton, "The phasor approach to fluorescence lifetime imaging analysis," Biophys. J. **94**(2), L14–L16 (2008).
16. J. A. Palero, H. S. de Bruijn, A. van der Ploeg-van den Heuvel, H. J. C. M. Sterenborg, and H. C. Gerritsen, "In vivo nonlinear spectral imaging in mouse skin," Opt. Express **14**(10), 4395–4402 (2006).
17. C. Buschmann and H. K. Lichtenthaler, "Principles and characteristics of multi-colour fluorescence imaging of plants," J. Plant Physiol. **152**(2-3), 297–314 (1998).
18. S. Meyer, A. Cartelat, I. Moya, and Z. G. Cerovic, "UV-induced blue-green and far-red fluorescence along wheat leaves: a potential signature of leaf ageing," J. Exp. Bot. **54**(383), 757–769 (2003).
19. R. Cisek, L. Spencer, N. Prent, D. Zigmantas, G. S. Espie, and V. Barzda, "Optical microscopy in photosynthesis," Photosynth. Res. **102**(2-3), 111–141 (2009).
20. E. M. M. Manders, F. J. Verbeek, and J. A. Aten, "Measurement of co-localization of objects in dual-colour confocal images," J. Microsc. **169**(3), 375–382 (1993).
21. F. Fereidouni, A. Esposito, G. A. Blab, and H. C. Gerritsen, "A modified phasor approach for analyzing time-gated fluorescence lifetime images," J. Microsc. **244**(3), 248–258 (2011).
22. H. Shirakawa and S. Miyazaki, "Blind spectral decomposition of single-cell fluorescence by parallel factor analysis," Biophys. J. **86**(3), 1739–1752 (2004).
23. I. T. Jolliffe, *Principle Component Analysis* (Springer Verlag, 1986).

1. Introduction

Fluorescence microscopy is commonly used to study (co)localization of multiple components in biological specimen [1]. These components can be distinguished by their spectroscopic properties, and simultaneously imaged by for instance (hyper) spectral imaging (SI) [2, 3], fluorescence lifetime imaging (FLIM) [4–7], or combinations of these techniques. Fluorescence lifetime imaging is typically employed to image molecular interactions on a nanometre scale by means of monitoring Förster Resonance Energy Transfer (FRET) [8], spectral imaging is the preferred way to study colocalization of multiple fluorophores on a pixel scale. Moreover, identification of endogenous fluorophores in complex biological samples can be performed by spectral imaging [9, 10] and spectral imaging of environment sensitive probes can be used to probe e.g. polarity, pH and Calcium concentration at a subcellular level. The major disadvantage of spectral imaging is that it requires complex analysis algorithms. Emission spectra are often broad and extend into multiple spectral channels. For spectral unmixing, the individual contributions of the fluorescent components to the total signal should be extracted from the data [2, 3]. Linear unmixing can be employed where the recorded spectra are mathematically unmixed using a number of fixed reference spectra of pure components [3]. The reference spectra are usually based on literature data or obtained in separate reference measurements. The use of such reference spectra can easily introduce artefacts because of changes in the spectra caused by solvatochromic shifts or other environmental effects. To correct for these effects, extensive calibration efforts are required.

Therefore, there is great interest in analysis routines that simplify analysis of spectral imaging data. An interesting recent development is the nonnegative matrix factorization algorithm for spectral imaging [11]. In the current work, we investigate the possibility to use phasor analysis for spectral imaging data. Phasor based image analysis has been shown to be very valuable for frequency domain [5, 12–14] and time domain [15] lifetime imaging data. The advantage of these approaches is that they are based on global analysis of the image data and that no (or limited) reference information is required. The spectral phasor analysis method presented here, is based on representing the spectra by phasors (polar representation). The spectra of individual pixels are Fourier transformed and the real and imaginary parts of the first harmonic are employed as coordinates in a phasor scatter plot. In this paper we show that the phasor representation of spectral data affords rapid and reliable unmixing of individual components in the image. To demonstrate the power of this approach, we unmix spectral images of cells stained with three fluorescent probes without the use of reference spectra. In addition, we unmix unknown auto fluorescent components in a grass blade. In the latter case, three autofluorescent components are identified and unmixed without prior knowledge of the autofluorescence composition

#164083 - $15.00 USD Received 5 Mar 2012; revised 11 Apr 2012; accepted 11 Apr 2012; published 22 May 2012

2. Materials and methods

2.1 Instrument details

The nonlinear spectral imaging microscope that is used to record the images is described in a previous paper [9, 10]. Briefly, the excitation light source consists of a mode-locked Titanium: Sapphire (Ti:Sa) laser (Tsunami, Spectra-Physics, Sunnyvale, CA) that tuned to 760 nm. The laser light is scanned in the XY direction using a galvanometer mirror scanner (040EF, LSK, Stallikon, Switzerland). In addition, the microscope is equipped with a Z-piezo objective translation stage (Mad City Labs, Madison, WI, USA) for adjusting the focus position. The laser light is focused on the sample by a microscope objective and the fluorescence emission is collected by the same objective lens. The results reported here are acquired using an infinity-corrected water-immersion objective (CFI Fluor 40xW, NA = 0.8, Nikon, Japan) with a long working distance (2 mm). The emission passes through a dichroic mirror (680 nm shortpass) and is filtered by a multiphoton emission filter (FF01-680/SP-25, Semrock, Rochester, NY, USA). The spectrograph consists of a fused silica equilateral dispersive prism (Linos, Göttingen, Germany), a focusing lens (f = 90 mm) and an EMCCD camera (Cascade 128 + EMCCD, Photometrics, Tucson, AZ, USA). A low level camera readout script and a customized driver are used for speed optimized camera performance. The images presented here are recorded at room temperature using a pixel dwell time of 128 µs. All raw images have a size of 70x70 µm (unless stated otherwise), 224 × 224 pixels and contain 128 wavelength channels for each pixel. A background spectrum for each pixel is simultaneously recorded with the emission spectra. The acquisition time for one image amounts to about 6.5 seconds.

2.2 Spectral phasor analysis

Spectral phasor analysis bears many similarities with fluorescence lifetime phasor analysis which is a well-known global analysis method for the analysis of fluorescence lifetime images [15]. In spectral phasor analyses, the fluorescence emission spectra of each and every pixel in the image are reduced to a "phasor" that is made up out of two numbers: the real and imaginary parts (amplitude and phase respectively) of the first harmonic of the Fourier transform of the fluorescence spectra. These two numbers are used as coordinates in a scatter plot, the phasor plot. Often, the phasor plots contain clouds of points that correspond to pixels with similar emission spectra. Selected regions in the phasor plot can be remapped to the original fluorescence image, thus providing segmentation based on pixels with similar spectral properties. Figure 1(a). illustrates how (Gaussian) reference spectra are mapped onto the phasor plot. The grid in the figure covers emission maxima over the spectral range 370 – 650 nm, in 10 nm steps and the spectral widths vary from 500 – 4000 cm^{-1} in steps of 500 cm^{-1}. For a fixed spectral width, the positions of the emission maxima lie on an arc; for clarity the wavelengths of the emission maxima are indicated by their colour.One of the advantages of the phasor representation is that it allows for fast, vector based mathematical operations. It enables rapid spectral unmixing, without the need for accurate reference spectra or elaborate fitting procedures.The spectral images can be represented as a three dimensional data set (X, Y, λ). In our setup, 128 wavelength channels are employed, but the analysis can also be performed on images with a much lower number of spectral channels, see Section 3.4. For each pixel (j) in a spectral image, the measured spectrum is considered to be a linear combination of the spectra of the fluorophores present in the detection volume. This assumption is valid only when the fluorophores are not subject to (interaction) effects such as solvatochromic shifts. The intensity y of a pixel with index j in wavelength channel n is related to the "concentration" X of fluorophore number k by:

$$y_{nj} = \sum_{n} a_{nk} x_{kj}. \qquad (1)$$

#164083 - $15.00 USD Received 5 Mar 2012; revised 11 Apr 2012; accepted 11 Apr 2012; published 22 May 2012

where a_{nk} is the fractional contribution to the intensity of spectrum k at wavelength channel n. For three components Eq. (1) reduces to:

$$y_{nj} = a_{n1}x_{1j} + a_{n2}x_{2j} + a_{n3}x_{3j}. \quad (2)$$

This is a linear set of equations, where each spectrum (a_{n1}, a_{n2} and a_{n3}) is normalized to one.

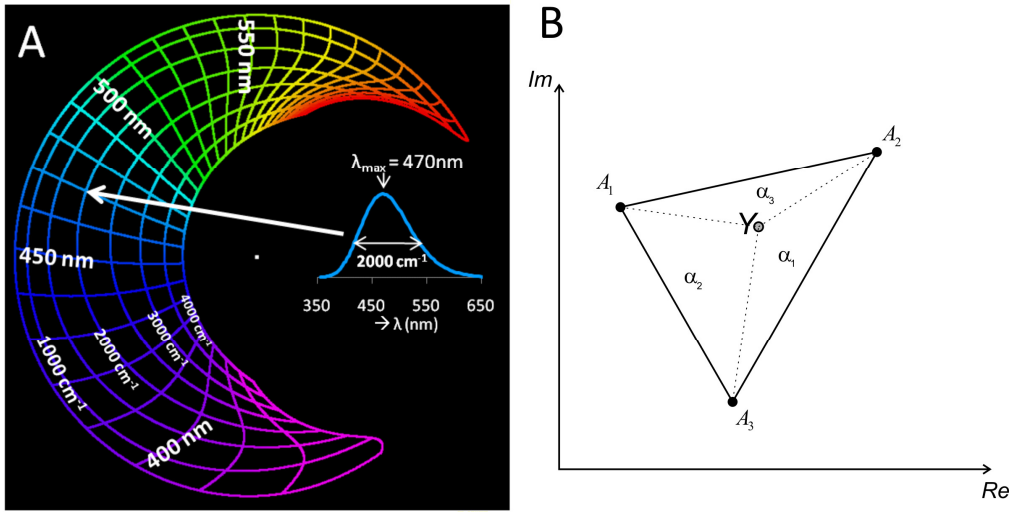

Fig. 1. (A) Reference spectral phasor plot showing the positions of Gaussian spectra. The grid covers emission maxima from 370 – 650 nm (the wavelength determines the position on the semicircle, as indicated by its colour) and spectral widths from 500 – 4000 cm^{-1} (with increasing spectral width, the position in the phasor plot is shifted towards the centre of the circle). As an example, a spectrum and its position in the phasor are shown. (B) The relative intensities α_1, α_2 and α_3 of components A_1, A_2 and A_3 in a pixel can be derived from the phasor.

When the spectra of the individual dyes are known, this linear system can be solved and concentrations of the individual components are obtained. This method, generally referred to as linear unmixing, allows for spectral unmixing of images and yields concentration maps of individual components [2].The number of components that can be unmixed is in principle unlimited but in practice restricted by the signal-to-noise ratio. Alternatively, unmixing can be achieved by fitting the spectrum with e.g. multiple Gaussian functions that resemble the spectra of the fluorescent components. After multiple iterations, the contributions of the individual components are obtained [16].

Spectral phasor analysis enables straight-forward unmixing of a mixture of three spectra. Consider the Fourier transformation of the spectrum *Yj*:

$$Y_j = \frac{A_1x_{1j} + A_2x_{2j} + A_3x_{3j}}{x_{1j} + x_{2j} + x_{3j}} = \alpha_1A_1 + \alpha_2A_2 + \alpha_3A_3. \quad (3)$$

With A_k the discrete Fourier transform of a_k at the first harmonic (the phasors of the spectra):

$$A_k = \sum_{n=1}^{N} a_{nk} e^{-i\frac{2\pi}{N}n}. \quad (4)$$

here N is the number of spectral channels and α_k the fractional intensity of component k which is defined as:

#164083 - $15.00 USD Received 5 Mar 2012; revised 11 Apr 2012; accepted 11 Apr 2012; published 22 May 2012

$$\alpha_k = \frac{x_k}{x_1 + x_2 + x_3}, \tag{5}$$

We note that normalization requires that α1 + α2 + α3 = 1. Therefore α3 can be replaced by 1 - (α1 + α2) resulting in:

$$Y_j = \alpha_1 A_1 + \alpha_2 A_2 + (1 - (\alpha_1 + \alpha_2)) A_3. \tag{6}$$

The real and imaginary parts of *Yj* can be written as:

$$\begin{aligned} \mathrm{Re}\, Y_j &= \alpha_1 \,\mathrm{Re}\, A_1 + \alpha_2 \,\mathrm{Re}\, A_2 + (1 - (\alpha_1 + \alpha_2)) \,\mathrm{Re}\, A_3, \\ \mathrm{Im}\, Y_j &= \alpha_1 \,\mathrm{Im}\, A_1 + \alpha_2 \,\mathrm{Im}\, A_2 + (1 - (\alpha_1 + \alpha_2)) \,\mathrm{Im}\, A_3, \end{aligned} \tag{7}$$

Solving *α1* and *α2* results in:

$$\begin{aligned} \alpha_1 &= \frac{\mathrm{Re}\, A_2 \,\mathrm{Im}\, Y - \mathrm{Re}\, Y \,\mathrm{Im}\, A_2 + \mathrm{Re}\, A_3 \,\mathrm{Im}\, A_2 - \mathrm{Re}\, A_2 \,\mathrm{Im}\, A_3 + \mathrm{Re}\, Y \,\mathrm{Im}\, A_3 - \mathrm{Re}\, A_3 \,\mathrm{Im}\, Y}{\mathrm{Re}\, A_2 \,\mathrm{Im}\, A_1 - \mathrm{Re}\, A_1 \,\mathrm{Im}\, A_2 - \mathrm{Re}\, A_3 \,\mathrm{Im}\, A_2 - \mathrm{Re}\, A_2 \,\mathrm{Im}\, A_3 + \mathrm{Re}\, A_1 \,\mathrm{Im}\, A_3 - \mathrm{Re}\, A_3 \,\mathrm{Im}\, A_1}, \\ \alpha_2 &= \frac{\mathrm{Re}\, A_3 \,\mathrm{Im}\, Y - \mathrm{Re}\, Y \,\mathrm{Im}\, A_3 + \mathrm{Re}\, A_1 \,\mathrm{Im}\, A_3 - \mathrm{Re}\, A_3 \,\mathrm{Im}\, A_1 + \mathrm{Re}\, Y \,\mathrm{Im}\, A_1 - \mathrm{Re}\, A_1 \,\mathrm{Im}\, Y}{\mathrm{Re}\, A_2 \,\mathrm{Im}\, A_1 - \mathrm{Re}\, A_1 \,\mathrm{Im}\, A_2 - \mathrm{Re}\, A_3 \,\mathrm{Im}\, A_2 - \mathrm{Re}\, A_2 \,\mathrm{Im}\, A_3 + \mathrm{Re}\, A_1 \,\mathrm{Im}\, A_3 - \mathrm{Re}\, A_3 \,\mathrm{Im}\, A_1}. \end{aligned} \tag{8}$$

with α3 = 1-(α1 + α2).

Plotting the phasors (imaginary versus real part) of A_k for k = 1, 2, 3, results in a triangle in the phasor plot with vertices at A_1, A_2 and A_3 (Fig. 1(b)). The phasor of a spectrum consisting of a linear combination of three pure components falls inside this triangle and the fractional intensities of the components are given by Eq. (8). Closer examination of Eq. (8) shows that α_1, the fractional intensity of component A_1, is equal to the area of the triangle formed by the phasor's position in the phasor plot (indicated by Y in Fig. 1(b)) and the two reference points A_2 and A_3 divided by the area of the reference triangle (A_1, A_2, A_3). To illustrate this consider two extreme cases: (1) when the measured point coincides with A_1, α_1 occupies the whole reference triangle and is therefore equal to one, and (2) when the measured point lies on the line connecting A_2 and A_3, α_1 will be zero. The fractional intensities of the other components are obtained in a similar way. We note that images of the unmixed intensities of individual components k are obtained by multiplying the α_k image with the (mixed) total intensity image.

2.3 Sample details

10 µM aqueous solutions were prepared from the fluorescent dyes Coumarin 120 (Sigma-Aldrich A9891), Rose Bengal (Sigma-Aldrich R3877) and Fluorescein (Sigma-Aldrich F6377). FluoCells prepared slide #2 (Invitrogen F-14781) contains bovine pulmonary artery endothelial cells (BPAEC). Texas Red-X phalloidin is labelling the F-actin, anti—bovine α-tubulin mouse monoclonal antibody in conjunction with BODIPY FL goat anti—mouse IgG antibody is labelling microtubules, and DAPI is labelling the nucleus. FluoCells prepared slide #6 (Invitrogen F-35925) contains fixed, permeabilized, and labelled muntjac skin fibroblast cells. Mitochondria are labelled with mouse anti–OxPhos Complex V inhibitor protein antibody and visualized using orange-fluorescent Alexa Fluor 555 goat anti–mouse IgG antibody. F-actin is labelled with green-fluorescent Alexa Fluor 488 phalloidin, and the nucleus is stained with TO-PRO-3 iodide. The grass blade sample was freshly picked near the laboratory and put in water to match the refractive index of the objective.

#164083 - $15.00 USD Received 5 Mar 2012; revised 11 Apr 2012; accepted 11 Apr 2012; published 22 May 2012

3. Results

3.1 Spectral phasor analysis of dye solutions

To demonstrate and explain the capability of spectral phasor analysis for segmenting fluorescence images, spectral images of three aqueous fluorescent dye solutions (Coumarin 120, Rose Bengal and Fluorescein are recorded and analysed, see Figs. 2(a)-2(c). The colour of the pixels in the phasor plot corresponds to the colour of fluorescence emission in that pixel as perceived by eye (real colour visualization [16]). For reference purposes a semicircle of theoretical Gaussian emission spectra with maxima ranging from λ_{em} = 370 to 650 nm and width $\Delta\lambda$ = 250 cm^{-1} is shown in the phasor plot. For images of solutions containing only a single dye, the positions of the phasors in the phasor plot are well localized; see the clouds of points in Figs. 2(a)-2(c). Examples of single-pixel spectra (coloured curves) from arbitrarily chosen pixels, as well as spectra averaged over the whole image (white curves), are shown in

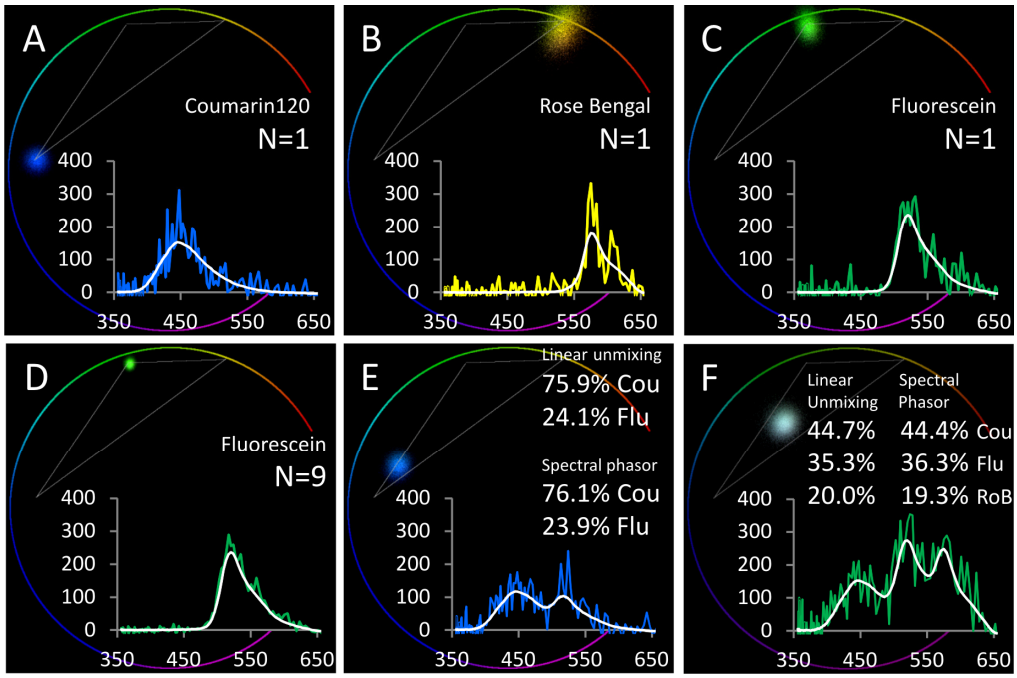

Fig. 2. Spectral phasor analysis of solutions of organic dyes Coumarin 120 (A), Rosebengal (B) and Fluorescein (C-D), mixtures of Coumarin 120 and Fluorescein, and a mixture of Coumarin 120, Fluorescein and Rosebengal (F). In each phasor diagram also the average spectrum over the whole image (white line) and of a single pixel is displayed (coloured line). A reference semicircle of Gaussian spectra (370-650 nm, 500 cm^{-1}) and a grey triangle connecting the reference positions of the dyes are indicated in each phasor diagram. We note that positions in the phasor plot are colour coded according to their real RGB colour.

the phasor plots. In typical imaging experiments, tens to hundreds of dye molecules are present in the focus of the microscope which results in noisy single pixel emission spectra. For the images used in Figs. 2(a)-2(c), we estimate that several hundred photons are detected per spectrum per pixel. For this signal level, the signal-to-noise ratio (S/N) at the emission maximum is approximately three. The size of the phasor cloud in Figs. 2(a-c) is determined by photon statistics and amounts to approximately 10-20 nm by 500-1000 cm^{-1}, which suggests that this signal level is sufficient to segment two components with a either a difference in emission maximum of >20 nm or a difference in spectral width of >1000 cm^{-1}. The size of the phasor cloud is reduced when spectral images are binned. The effect of binning 3x3 pixels (N = 9) is shown for Fluorescein in Fig. 2(d). Binning results in a narrower

#164083 - $15.00 USD Received 5 Mar 2012; revised 11 Apr 2012; accepted 11 Apr 2012; published 22 May 2012

distribution of the phasor points; here the size of the phasor cloud is reduced to ~5 nm by ~500 cm^{-1}. The higher signal level clearly affords separating smaller spectral differences.

The spectral phasor approach enables convenient spectral unmixing of mixtures of fluorophores based on Eq. (8). This is exemplified in Figs. 2(e)-2(f), where phasors of (homogeneous) mixtures of Coumarin 120 and Fluorescein (E) and of Coumarin 120, Fluorescein and Rose Bengal (F) are shown. Conventional linear unmixing of the average spectrum of the Coumarin and Fluorescein image results in relative contributions of 75.9% and 24.1%, respectively. This is in excellent agreement with the phasor unmixing results of 76.1% and 23.9% (Fig. 2(e)). The results for the unmixing of the mixture of Coumarin 120, Fluorescein and Rose Bengal are again in excellent agreement. Linear unmixing yields relative contributions of 44.7%, 35.3% and 20%, respectively; spectral phasor unmixing yields contributions of 44.4%, 36.3% and 19.3%, respectively.

3.2 Spectral phasor based unmixing of labeled cells

To further evaluate the capability of spectral phasor analysis to unmix spectral images, we analysed spectral images of Molecular Porbe FluoCells test slide #2 and #6. The fluorescent dyes in these specimens can be simultaneously excited by two-photon excitation at 790 nm. Figure 3 summarizes the phasor analysis of a single cell on the test slide#2. In Fig. 3(b) the "real colour RGB" fluorescence image [16] of the cell is shown. Figure 3(a) shows the phasor plot of the cell. For unmixing, reference phasor positions should be identified to construct the triangle discussed in Fig. 0.2(b). Ideally, reference phasors are obtained from areas in the specimen that contain only a single fluorescent component. Such references may be found at the edges of the phasor distribution. To verify whether these edges indeed correspond to "pure" components, the spectra from the selected areas in the phasor diagram (indicated by the dashed boxed areas) are shown in Fig. 3(a). The spectra are clearly not pure, but do reveal clear emission maxima from the three dyes. The spectra in Fig. 3(a). reveal that there are pixels that contain only Texas Red or DAPI but pixels containing BODIPY (white box) always contain a significant contribution of Texas Red. Consequently, the phasor cloud does not extend to the BODIPY reference point. Therefore, in Fig. 3(a) phasor reference *curves* are added for each dye. The curves are constructed using Gaussian shaped emission spectra with the experimentally determined maximum emission wavelengths of the dyes (DAPI λ_{em} = 460 nm, BODIPY λ_{em} = 525 nm and Texas Red λ_{em} = 615 nm) and a spectral width that varies between 250 and 3000 cm^{-1}. The reference points can now be estimated by extrapolating the phasor clouds to the three reference curves. Spectral unmixing based on these reference phasors yields excellent results on this test specimen. The signal of DAPI (nucleus) is accurately separated from the Texas Red (actin) and BODIPY (tubulin) signals; also the latter two are remarkably well unmixed with no detectable bleed through, see Figs. 3(c)-3(e) sample 1. The same approach is applied to the test slide #6. The emission maxima for Alexa 488, Alexa 555 and TO-PRO-3 are again derived from selected areas in the phasor diagram. Next, the three reference curves are drawn for these maxima. Again clear segmentation without bleeding through of actin, mitochondria and nucleus is achieved (Fig. 4(c)-4(e)).The images of Figs. 3 and 4 are also analysed using the Nonnegative Matrix Factorization algorithm introduced by Neher *et al* [11]. Independent of their 'segregation bias' some spectral bleed through is observed. Input of approximate reference spectra is required to correctly unmix the image with minimal bleed through (not shown).

#164083 - $15.00 USD Received 5 Mar 2012; revised 11 Apr 2012; accepted 11 Apr 2012; published 22 May 2012

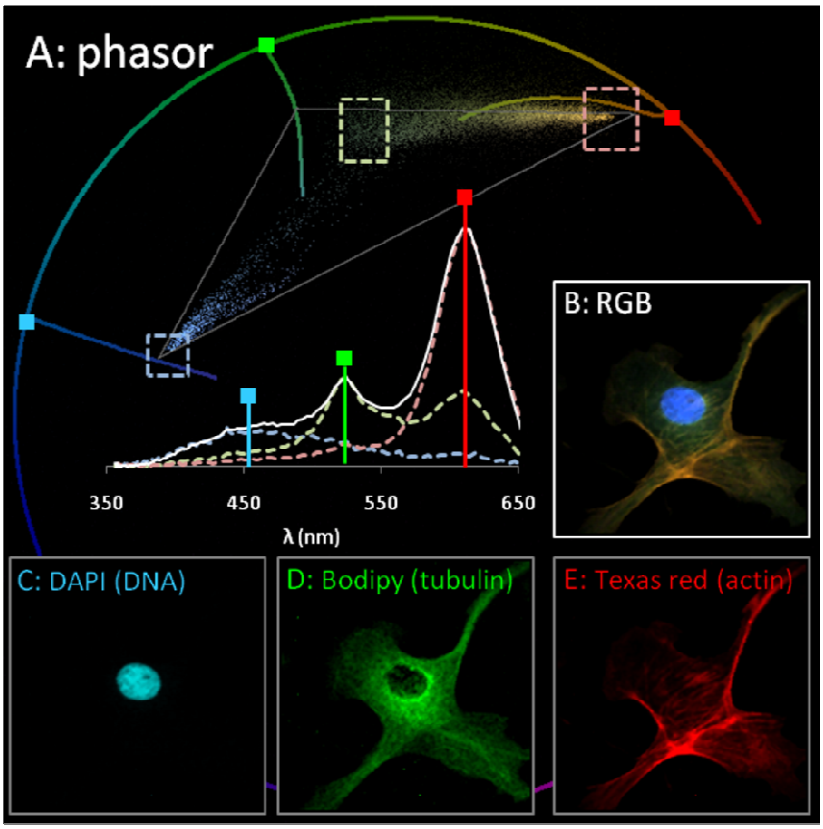

Fig. 3. Spectral phasor analysis of FluoCells test slides #2 (field of view 80x80µm) A) Spectral phasor plot; for three areas in the phasor plot (indicated by the dashed boxes), the spectra are averaged and displayed together with the average spectrum of the whole image. A solid reference semicircle (370-650 nm, 500 cm^{-1}) and three solid reference lines corresponding to the positions of the emission maxima found from the spectra are shown in the phasor plot. B) Real colour representation of the original image. C-E) Unmixed images of DAPI, BODIPY and Texas Red.

3.3 Unmixing of autofluorescence in grass blade

The analysis of specimens containing endogenous (autofluorescent) fluorophores can be challenging, especially when their origin and spectral characteristics are not known. To exemplify the analysis of an unknown biological specimen, a multiphoton spectral image of the autofluorescence of a randomly picked grass blade is analysed. The spectral phasor plot and RGB fluorescence image of the grass blade are shown in Figs. 5(a)-5(b). The blue/green fluorescence mainly originates from hydroxycinnamic acids and/or flavonoids [17,18], whereas the red emission is mainly from chlorophylls [19]. The distribution of the points in the phasor plot is triangularly shaped and the average spectra near the edges of the triangle (taken from the areas indicated by the dashed squares) reveal that the blue and red components have their main emission maxima at 470 nm and 635 nm respectively. The main peak of the green emission is at 495 nm, but a strong second peak is also observed at approximately the same wavelength as the red emission. Clearly, the image does not contain pixels that contain pure green emission. For the spectral unmixing of this specimen, reference phasors lines corresponding to the locations of the emission maxima (λ_{em} = 470 nm for the blue, λ_{em} = 495 nm for the green and λ_{em} = 635 nm for the red component) and a range of spectral widths (from 250 and 3000 cm^{-1}) are drawn into the phasor plot. The edges of the solid triangle in Fig. 5(a) are found by extrapolating the phasor clouds manually. Figures 5(c-

#164083 - $15.00 USD Received 5 Mar 2012; revised 11 Apr 2012; accepted 11 Apr 2012; published 22 May 2012

5(e) shows the spectrally unmixed components of the grass blade. Again the spectrally unmixed images are of good quality and no obvious bleed through is observed between the different components.

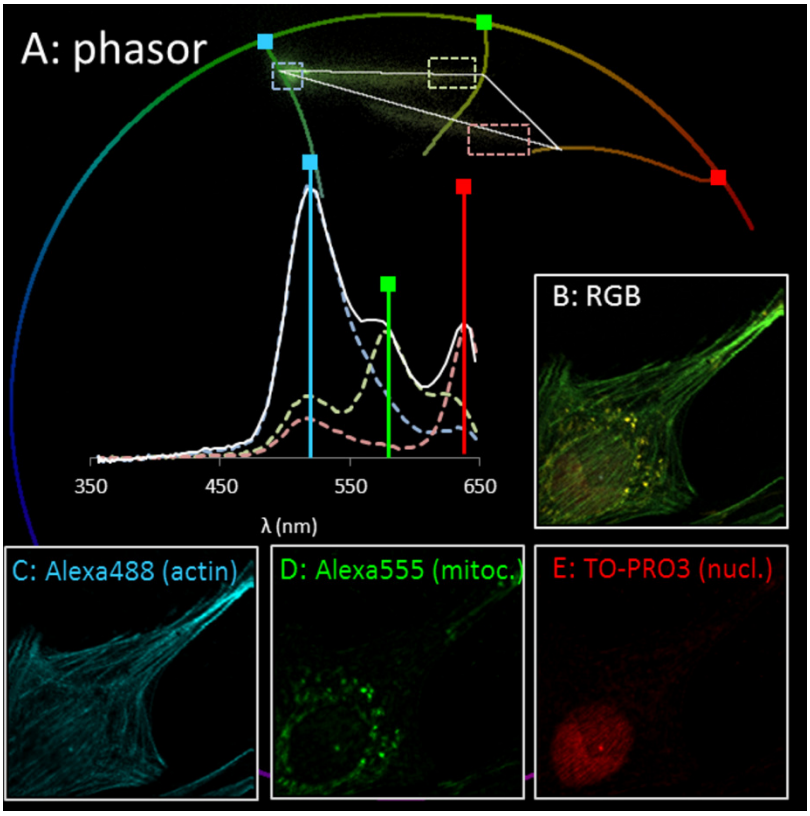

Fig. 4. Spectral phasor analysis of FluoCells test slides #6 (field of view 50x50µm); A) Spectral phasor plot; for three areas in the phasor plot (indicated by the dashed boxes), the spectra are averaged and displayed together with the average spectrum of the whole image. A solid reference semicircle (370-650 nm, 500 cm^{-1}) and three solid reference lines corresponding to the positions of the emission maxima found from the spectra are shown in the phasor plot. B) Real colour representation of the original image. C-E) Unmixed images of Alexa 488, Alexa 555 and TO-PRO3.

3.4 Compatibility of spectral phasor analysis with other (hyper-) spectral imaging systems

The spectral images employed in the above examples were recorded using a spectrograph with 128 wavelength channels per pixel. This system has a sufficiently high spectral resolution to determine the emission maxima and spectral widths. Most commercial spectral imaging systems are based on (multi-anode) photo multiplier tubes. Typically, they are equipped with a 32, 16, 8 or 4 detection channels. To investigate the effect of the number of spectral channels on phasor based segmentation we calculated phasor plots of Gaussian reference spectra for imaging systems with 16, 8 and 4 detection channels (see Figs. 6(a), 6(b), 6(c)). The raster patterns in Fig. 6 correspond to emission wavelength steps of 10 nm and spectral width steps of 500 cm^{-1} (similar to Fig. 1(a)). At 16 channels the raster pattern is unaffected by the reduction of the number of channels; at 8 channels, however, the pattern is distorted in particular for narrow spectra (<1000 cm^{-1}). For 4 channels the distortion of the pattern is even more severe. Next, the spectral image shown in Fig. 3 is re-binned to 4, 8 and 16 spectral channels (linear with wavelength) and represented in spectral phasor plots (see Figs. 6(a), 6(b), 6(c)). Interestingly, the spectral unmixing is not affected by the reduction in

#164083 - $15.00 USD Received 5 Mar 2012; revised 11 Apr 2012; accepted 11 Apr 2012; published 22 May 2012

the number of spectral channels. To quantify the similarity between the spectrally unmixed images, Manders overlap coefficients are calculated [20]. The value of this coefficient ranges from 0 to 1, with 1 indicating perfect overlap and zero indicating no overlap of the two images. For convenience the three unmixed images are stitched together to be able to calculate a single Manders coefficient per set of unmixed images. Next, the Manders coefficients for 128, 16, 8 and 4 channel unmixing are calculated.

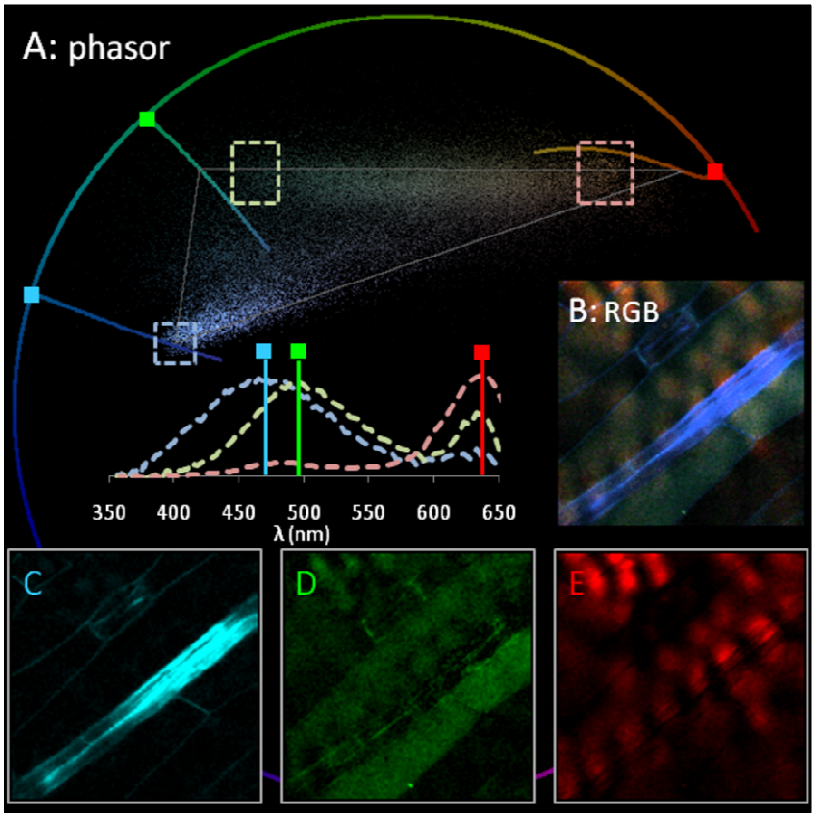

Fig. 5. Spectral phasor plot of a Grass blade autofluorescence image. For three areas in the phasor plot, the spectra are averaged and displayed (indicated by dashed boxes and spectra) together with the average spectrum of the whole image. A solid reference semicircle of Gaussian spectra (370-650 nm, 500 cm^{-1}) and three solid reference lines of the positions of emission maxima found in the spectra (470 nm, 495 nm and 630 nm) are also shown. The grey triangle connects the reference positions of the dyes, allowing unmixing of the image in the three channels. B) The real colour representation of the autofluorescence image. C-E) The unmixed signals.

Here, the 128 channel value (original Fig. 3) serves as a reference. In all cases the Manders coefficient is between 0.97 and 0.98, indicating almost perfect overlap. For comparison, images corresponding to three spectrally filtered emission windows (420-480nm for DAPI, 500-550nm for BODIPY and 580-650 for Texas Red) are constructed from the 128 channel spectral data (see Fig. 6(d)).

In this case (no unmixing), strong bleed through of DAPI into the green channel is observed. When comparing these images (again stitched) to the 128 channel phasor unmixing result the overlap is considerably reduced, the Manders coefficient amounts to 0.87.

At 4 wavelength channels, the phasor based spectral unmixing requires prior knowledge of the emission maxima of the dyes. Here, the low spectral resolution does not allow establishing the positions of the emission maxima. Consequently it is not possible to construct reference

#164083 - $15.00 USD Received 5 Mar 2012; revised 11 Apr 2012; accepted 11 Apr 2012; published 22 May 2012

phasor lines for the emission maxima. At least 8 channels are required to obtain sufficient information to construct the reference phasor lines.

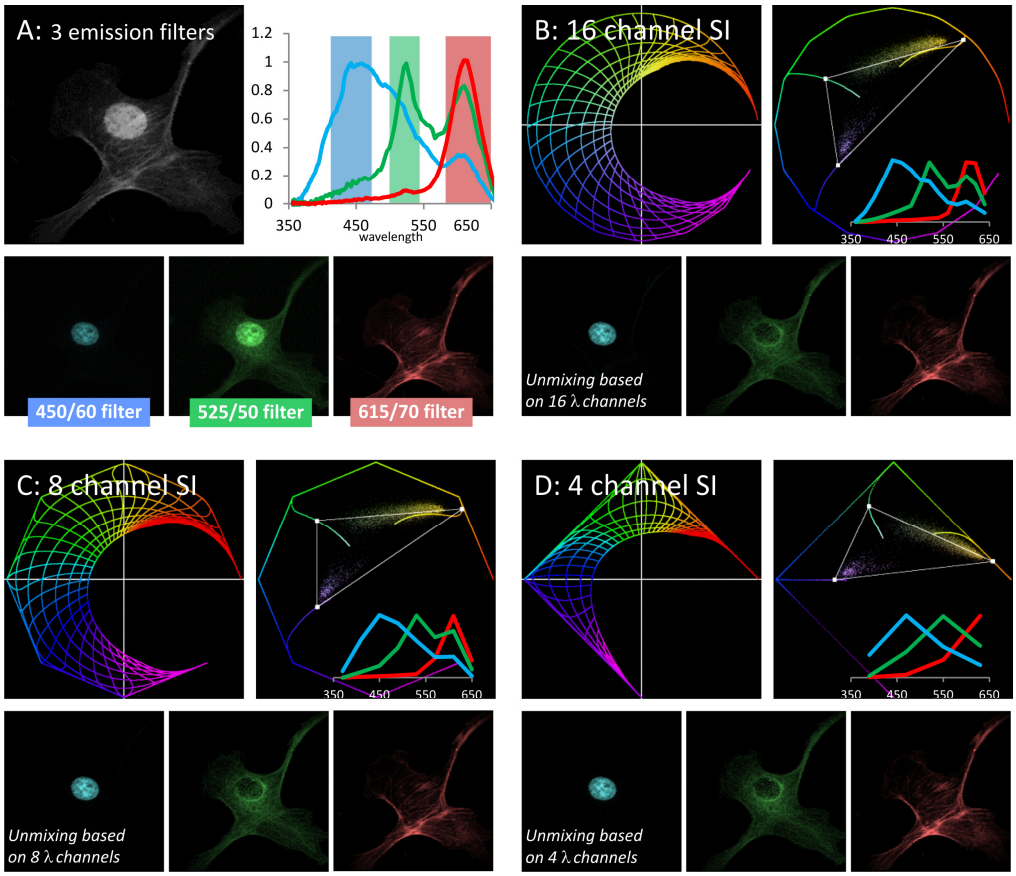

Fig. 6. Spectral analysis of the BPAE cells shown in Fig. 3. (A) Images corresponding to 3 emission filters (top) and total intensity (bottom). (B-D) Spectral phasor diagrams of spectral images with 16, 8 and 4 wavelength channels respectively. The reference phasor grids (top left) cover emission maxima from 370 – 650 nm and spectral widths from 500 – 4000 cm^{-1}. Spectra of regions at the edges of the phasor cloud are included.

4. Discussion

In this work, it is demonstrated that phasor analysis can be applied to spectral imaging data. Here, similar to phasor analysis of time-domain lifetime imaging, the Fourier transform representation is used for visualization and analysis of the image data. Fourier transformation results in a spectrum of harmonics and the phasor plots are constructed by employing the real and imaginary components of the first harmonic of the transform as X and Y coordinates in a scatter plot. Spectral phasor analysis is a fast and photon efficient way to extract two characteristic numbers from a spectrum that are related to the maximum wavelength and width of the spectrum. In principle also the higher harmonics can be employed to construct phasor plots. However, the first harmonic has the highest amplitude and is therefore least sensitive to noise. Closer examination of Eq. (7) reveals that it is not possible to unmix more than 3 components. A sample with 4 components requires estimating 3 unknown parameters (α_1, α_2 *and* α_3) while the number of equations is limited to two. Including the additional information that the higher order harmonics provide might enable the unmixing of more than three components. This is possible due to the orthogonality of the Fourier components which allows adding additional dimensions to the phasor plot and extending it into a 3D histogram.

#164083 - $15.00 USD Received 5 Mar 2012; revised 11 Apr 2012; accepted 11 Apr 2012; published 22 May 2012

However, analysis of this 3D cloud is not trivial. The development of an algorithm that automatically finds the reference points is under consideration.

In the phasor unmixing we employ Gaussian reference curves generated by varying the widths of Gaussian shaped spectra. These curves serve as guidelines to assign the reference points for samples where the vertices of the phasor plot are not clearly visible. Assuming a different shape for the reference spectra introduces a small shift in the positions of the reference curves. However, in our experience the choice of the reference points is not very critical; variations of the reference points have only small effects on the accuracy of the unmixing.

The spectral phasor offers similar capabilities for image analyses as the lifetime phasor [14], but now based on spectral properties. Phasor plots can be employed for segmentation since image pixels mapped onto the same position in the phasor plot have similar widths and maximum wavelengths [21]. Images can be unmixed and in addition information is available about the heterogeneity in the pixel composition. Spectral phasor analysis does not require extensive calibration. In this work the Fourier transformation is carried out on uncalibrated spectra. The spectral range of 350 to 700 nm is detected by a 128 channel spectrograph. Because of the nonlinear dispersion of the prism, the channel numbers are not linear with wavelength (from ~2 nm/pixel at 400 nm to ~5 nm/pixel at 700 nm). On a wavenumber scale (energy), the scale is close to linear in the visible range (100-120 cm^{-1}/pixel). Moreover, at 655 nm the emission is cut off by an emission filter. All these factors influence the position of the measured spectrum in the phasor plot. Clearly, the use of other spectral detectors and microscopes will affect the phasor plot. This can be avoided by calibration of the wavelength scale and response of the spectral imaging system. There are several other unmixing methods that can be employed to separate the components in spectral images. Linear unmixing is the most common technique, it is straightforward and software is readily available. Importantly, linear unmixing requires accurate reference spectra of the individual components which is not straight-forward. Emission spectra often depend on the local environment of the dyes; the spectra in cells may very well differ from those in solution. This compromises the accuracy of linear unmixing. Several blind unmixing approaches were introduced to overcome these difficulties such as PARAFAC [22], principle component analyses (PCA) [23] and non-negative matrix factorization (NMF) [11]. PARAFAC is complicated by the fact that both excitation and emission spectra need to be measured. This makes the method fairly complicated and impractical for fluorescence microscopy. PCA is mathematically complicated and reveals the internal structure of the data in a way which best explains the variance in the data. One of the complications with this method is that it is sensitive to round-off errors and that noise in the images may result in negative contributions of components. These problems were mitigated in the NMF method which has been demonstrated to yield good results on spectral images of fluorescent cells with up to 4 labels. However, the NMF needs to be fed with approximate reference spectra that are modified during the unmixing procedure. Unfortunately, the unmixing result does depend on the initial value of the start spectra. The spectral phasor approach also requires reference values, but the phasor plot itself can provide these reference values. The phasor plot allows determination of the peak positions of the fluorescent molecules in their native environment. The results show improved unmixing results compared to linear and NMF based unmixing.

The most important advantage of the spectral phasor based unmixing compared to other approaches is that it is fast, robust and that reference phasors can be derived from the phasor plot. Creating a phasor plot of a 256x256 pixel image with 128 spectral channels takes about one second on a standard PC, much faster than the NMF method. However, so far no more than three components can be unmixed with the spectral phasor approach. We note that the time required to calculate the phasor plot is significantly reduced for lower numbers of spectral channels. One of the interesting features of the phasor approach is that areas selected in the phasor plot can be mapped back to the image to realize segmentation based on spectral

#164083 - $15.00 USD Received 5 Mar 2012; revised 11 Apr 2012; accepted 11 Apr 2012; published 22 May 2012

differences. In this way (many) more than 3 ‘components’ can be separated.Phasor based unmixing relies at present on the manual assignment of the positions of the reference points in the phasor plot. Nevertheless, it is easy to check whether suitable reference points have been chosen by determining the emission maxima of average spectra of selected regions in the vicinity of the anticipated reference point. Overall, spectral phasor analysis is a method to unmix spectral images with minimal input, and the input that is required can be obtained from the spectral image itself. The most important prerequisite is that the fluorescent dyes have emission maxima that can be extracted from the average spectrum of (part of) the image. For fluorescent labels, this is often the case, especially when the number of spectral channels is large. The examples in this paper show the power of the spectral phasor method: it facilitates rapid separation of the fluorescence components in images. Since it can be applied to most spectral imaging data, we believe that spectral phasor analysis is valuable tool for the analysis of spectral images.

An ImageJ plugin for spectral phasor analyses is available from the author’s web site.

#164083 - $15.00 USD Received 5 Mar 2012; revised 11 Apr 2012; accepted 11 Apr 2012; published 22 May 2012